

# Recovering the intrinsic shape of early-type galaxies

Remco C. E. van den Bosch<sup>1,2</sup>, Glenn van de Ven<sup>3\*</sup>

<sup>1</sup> *McDonald Observatory, The University of Texas at Austin, Austin, TX 78712, USA* [[bosch@astro.as.utexas.edu](mailto:bosch@astro.as.utexas.edu)]

<sup>2</sup> *Sterrewacht Leiden, Universiteit Leiden, Postbus 9513, 2300 RA Leiden, The Netherlands*

<sup>3</sup> *Institute for Advanced Study, Einstein Drive, Princeton, NJ 08540, USA* [[glenn@ias.edu](mailto:glenn@ias.edu)]

Accepted 2009 June 1. Received 2009 May 27; in original form 2008 November 20

## ABSTRACT

We investigate how well the intrinsic shape of early-type galaxies can be recovered when both photometric and two-dimensional stellar kinematic observations are available. We simulate these observations with galaxy models that are representative of observed oblate fast-rotator to triaxial slow-rotator early-type galaxies. By fitting realistic triaxial dynamical models to these simulated observations, we recover the intrinsic shape (and mass-to-light ratio), without making additional (ad-hoc) assumptions on the orientation.

For (near) axisymmetric galaxies the dynamical modelling can strongly exclude triaxiality, but the regular kinematics do not further tighten the constraint on the intrinsic flattening significantly, so that the inclination is nearly unconstrained above the photometric lower limit even with two-dimensional stellar kinematics. Triaxial galaxies can have additional complexity in both the observed photometry and kinematics, such as twists and (central) kinematically decoupled components, which allows the intrinsic shape to be accurately recovered. For galaxies that are very round or show no significant rotation, recovery of the shape is degenerate, unless additional constraints such as from a thin disk are available.

**Key words:** galaxies: elliptical and lenticular, cD - galaxies: kinematics and dynamics - galaxies: structure

## 1 INTRODUCTION

Numerical cold dark matter simulations predict that the dark matter haloes of galaxies typically have intrinsic shapes with three distinct axes  $a$ ,  $b$  and  $c$  (e.g. Jing & Suto 2002). Such a triaxial shape is characterized by the axis ratios  $p = b/a$  and  $q = c/a$  and  $0 \leq q \leq p \leq 1$ , which can vary as a function of radius. Based on the specific angular momentum inferred from integral-field stellar kinematics, early-type galaxies seem to be divided into two classes of fast and slow rotators, different from their morphological classification in ellipticals and lenticulars (Kormendy & Bender 1996; Emsellem et al. 2007). Most fast rotators, including lenticular as well as many elliptical galaxies, which show strong rotation around their photometric minor axis, seem consistent with oblate axisymmetry ( $p = 1$ ). However, many of these systems contain bars and also weakly triaxial shapes can not be ruled out. On the other hand, the slow rotators, with little or no rotation, are most likely triaxial.

However, all this is based on observed quantities, i.e., projected onto the plane of the sky, while for the true comparison between galaxies intrinsic properties, and thus the viewing directions are needed. Most early-type galaxies lack thin discs (in either dust, gas or stars), so that typically there is only a weak constraint on the viewing direction from (mainly) the observed ellipticity.

Determining the intrinsic shape of galaxies is possible by statistical analysis of their observed ellipticities (e.g. Lambas, Maddox & Loveday 1992; Ryden 1992). The deficiency of E0 type galaxies immediately rules out that elliptical are perfectly axisymmetric (Franx, Illingworth & de Zeeuw 1991; Ryden 1996), even if bars are taken into account. A recent study by Padilla & Strauss (2008) using ellipticities from SDSS show that early-type galaxies are weakly triaxial with mean axial ratios of  $p \sim 0.95$  and  $q \sim 0.7$ . However, these kind of analyses involve rather strong assumptions on the intrinsic shape distribution, and can not determine the shape of individual galaxies. Alternatively, by assuming a functional form for the intrinsic density it is possible to constrain the intrinsic shape of the light distribution of an individual galaxy, given its observed ellipticity and isophotal twist profile (e.g. Williams 1981; Chakraborty et al. 2008). In general, however, there is a well-known non-uniqueness in the deprojection of the surface brightness—even for axisymmetric galaxies not viewed perpendicular to their symmetry axis—also called the ‘cone of ignorance’ (Rybicki 1987). This tells us that it is not possible to constrain the intrinsic shape using only the photometry without making strong assumptions.

Nowadays, in addition to observations of the surface brightness of early-type galaxies, integral-field spectrographs provide the full line-of-sight velocity distribution (LOSVD) as a function of position on the sky  $\mathcal{L}(x', y', v_{z'})$ . The LOSVD is commonly parameterized in terms of its velocity moments, resulting in maps of

\* Hubble Fellow

the mean line-of-sight velocity, velocity dispersion and higher-order velocity moments. Can we (better) constrain the intrinsic shape, and hence the viewing direction, of galaxies from these two-dimensional photometric and kinematic observations?

Because the deprojection is degenerate and the conversion from light to mass is complicated when dark matter is present, implying a range of possible gravitational potentials. Even ignoring (or parameterizing) both these aspects, it is far from evident that the LOSVD provides enough information to infer the intrinsic shape. Let us first consider three-integral oblate axisymmetric models, i.e., with a distribution function (DF) that is a function  $f(E, L_z, I_3)$  of the energy  $E$ , the angular momentum component  $L_z$  parallel to the symmetry  $z$ -axis, and a non-classical third integral of motion  $I_3$ . In the special case that a galaxy happens to be well approximated by a two-integral DF  $f(E, L_z)$ , the density  $\rho(R, z)$  (in the cylindrical coordinates  $R$  and  $z$ ) uniquely determines the even part of  $f(E, L_z)$  and the mean streaming  $\rho\langle v_\phi \rangle$  in the meridional plane fixes the part of  $f(E, L_z)$  that is odd in  $L_z$  (Dejonghe 1986). If both  $\rho(R, z)$  and  $\rho\langle v_\phi \rangle$  are known, they define a two-integral DF completely. The observed velocity dispersion and higher order velocity moments of the LOSVD then provide additional information, which for example can be used to constrain the inclination (see e.g. Cappellari et al. 2006). This two-integral semi-isotropic result was recently generalized by Cappellari (2008) using a special class of anisotropic models in which the velocity ellipsoid is assumed to be aligned with cylindrical coordinates, and the anisotropy  $\beta_z$  (as defined by Binney & Mamon 1982) to be positive and constant within a galaxy. Both assumptions are based on a simplified interpretation of fig. 1 in Cappellari et al. (2006), and is at most a first-order approximation.

In the realistic case of a three-integral DF  $f(E, L_z, I_3)$ , it might well be that the full three-variable LOSVD  $\mathcal{L}(x', y', v_{z'})$  is needed to determine the DF, so that there is no information left to constrain the inclination. Using long-slit spectroscopy it was generally impossible to constrain the inclination (e.g. van der Marel et al. 1998; Gebhardt et al. 2000). Initially, the availability of two-dimensional stellar kinematics seem to allow a constraint on the inclination beyond the lower limit from the photometry, even in the case of full three-integral axisymmetric orbit-based Schwarzschild models (Verolme et al. 2002). However, Krajnović et al. (2005) convincingly showed that, after carefully taking into account numerical effects, similar three-integral axisymmetric Schwarzschild models at different inclinations above the photometric limit can (nearly) all fit the observed LOSVD within the measurement uncertainties.

Thomas et al. (2007) showed that axisymmetric modeling can have significant systematics in the recovered mass-to-light ratios by modelling triaxial merger remnants with their axisymmetric machinery. This shows that triaxial modelling is strongly preferred over axisymmetric modelling, as real elliptical galaxies are at least weakly triaxial.

In the triaxial case, the DF is again a function of three integrals of motion  $f(E, I_2, I_3)$ , but the orbital structure in these models is substantially richer than in the oblate axisymmetric models, with four major orbit families, instead of only one. This introduces a “fundamental” non-uniqueness in the recovery of the DF: whereas in the oblate axisymmetric case  $\rho(R, z)$  uniquely defines the even part of  $f(E, L_z)$ , in the (separable) triaxial case the density  $\rho(x, y, z)$  does *not* uniquely determine the even part of  $f(E, I_2, I_3)$ , even though both of these are functions of three variables (Hunter & de Zeeuw 1992). It is (yet) unknown how much specification of  $\mathcal{L}(x', y', v_{z'})$  can narrow down the range of possible DFs further. Therefore, in the triaxial case it seems to be even harder, if not impossible, to constrain the viewing direction.

However, while mathematically there are an infinite number of deprojections of the surface brightness possible already for oblate axisymmetric systems viewed away from edge-on, in practice only a limited range of deprojections lead to intrinsic density distributions that are considered realistic for galaxies. Similarly, we have shown in (van de Ven, de Zeeuw & van den Bosch 2008, hereafter vdV08) that the DF in the triaxial case is in practice well recovered at the correct viewing direction using orbit based models. At the same time, we found in (van den Bosch et al. 2008, hereafter vdB08) that if there is enough complexity in the photometry and/or kinematics it is likely that even the intrinsic triaxial shape is well constrained. Such complexities are for example photometric and kinematic twists, misalignment between the photometric minor axis and kinematic rotation axis (kinematic misalignment) and so-called kinematically decoupled components (KDCs). For example, the velocity field of NGC 4365 (Davies et al. 2001) shows rotation around the photometric short-axis in the core as well as around the long-axis in the outer parts. While the central KDC excludes a prolate shape, the global long-axis rotation is not possible in an oblate system, leaving a triaxial intrinsic shape as the only solution (see also vdB08).

Statistical analysis of observed ellipticities and kinematic misalignments can provide an estimate of the intrinsic shape distribution (Binney 1985; Franx et al. 1991). However, this statistical approach requires a large sample of galaxies for which the kinematic misalignment is accurately measured, which is not (yet) available. Tenjes et al. (1993) explored the use of the observed ellipticity and kinematic misalignment to constrain the intrinsic shape of individual galaxies, adopting a specific form for the intrinsic density and streaming motion. Statler (1994, and references therein) developed a velocity-field fitting method for individual galaxies based on a solution of the continuity equation, assuming a similar flow which separates the density and streaming motion in a radial and angular part. Because this approach is fast the large parameter space can be sampled finely enough to find the most probable solution using Bayesian statistics. However, the method assumes a (plausible) solution for the continuity equation, is not self-consistent, and fits the first velocity moment only. By comparison, the orbit-based Schwarzschild models that we employ allow for general density distributions, are self-consistent, and fit the full LOSVD. As mentioned above, even with such a general method making optimal use of the state-of-the-art two-dimensional photometric and kinematic observations, it is not evident how well the intrinsic shape can be recovered.

In this paper, we use a set of realistic (nearly) axisymmetric and triaxial galaxy models with a three-integral DF, to show that an increasing complexity in the corresponding two-dimensional observables indeed leads to a better recovery of the intrinsic shape. In § 2, we construct these Abel models based on the description of vdV08. We fit the corresponding observables using the triaxial Schwarzschild method of vdB08, of which we highlight the most relevant aspects in § 3. We investigate the resulting constraints on the intrinsic shape in § 4, and briefly discuss the recovery of the intrinsic moments in § 5. We discuss our findings and conclude in § 6.

## 2 GALAXY MODELS WITH A THREE-INTEGRAL DISTRIBUTION FUNCTION

Following vdV08, we build triaxial Abel models with a separable (or Stäckel) potential that are a generalization of the spherical Osipkov-Merritt (Osipkov 1979; Merritt 1985) models (see also Dejonghe & Laurent 1991; Mathieu & Dejonghe 1999). These models, with

a DF  $f(E, I_2, I_3)$  that depends on three exact integrals of motion, allow for a large range of shapes and internal dynamics, while the corresponding observables, including the LOSVD, can be computed efficiently. They are well suited to simulate realistic imaging and integral-field kinematics of early-type galaxies. Here, we construct thirteen galaxy models, six nearly oblate axisymmetric, three nearly prolate axisymmetric and four triaxial. These galaxy models are representative of early-type galaxies observed with the integral-field spectrograph SAURON (e.g. Emsellem et al. 2004), from oblate fast-rotator to triaxial slow-rotator.

As in § 4 of vdV08, we use a triaxial isochrone Stäckel potential with a length scale of  $10'' \simeq 1 \text{ kpc}$  at the adopted distance of 20 Mpc, and with a total mass of  $10^{11} M_\odot$ . Next, we choose the DF to be a linear combination of components of the form  $f(S) = (S - S_{\text{lim}})/(1 - S_{\text{lim}})$ , where both  $S = -E + wI_2 + uI_3$  and  $S_{\text{lim}}$  depend on the (constant) shape parameters  $w$  and  $u$ . Moreover, each DF component can be one of three types. The non-rotating (NR) type is made of box orbits and tube orbits with both senses of rotation populated equally. In addition we have two rotating types, long-axis rotating (LR) and short-axis rotating (SR), which consist of tube orbits, and have net rotation around the long axis and short axis respectively. We set  $u$  and  $w$  of each component such that the total density is similar to that corresponding to the potential, except in the outer parts ( $> 30''$ ) where a steeper surface brightness profile mimics the presence of dark matter (see also vdV08).

To calculate the observables we need to choose a viewing direction. For the oblate/prolate axisymmetric models we adopt three inclinations: close to edge-on/side-on  $i = 87^\circ$  ( $\cos i \simeq 0.05$ ), intermediate  $i = 60^\circ$  ( $\cos i = 0.50$ ), and close to face-on/end-on  $i = 18^\circ$  ( $\cos i \simeq 0.95$ ). For the triaxial models we use polar and azimuthal viewing angles of  $\vartheta = \varphi = 60^\circ$ . We then compute for each DF component on a rectangular grid on the sky plane the LOSVD and fit a Gauss-Hermite series to obtain maps of the surface mass density  $\Sigma$ , and the mean line-of-sight velocity  $V$ , velocity dispersion  $\sigma$  and higher-order Gauss-Hermite velocity moments up to  $h_6$  (Gerhard 1993; van der Marel & Franx 1993). The surface brightness is obtained from dividing  $\Sigma$  by a constant (total) mass-to-light ratio  $M/L = 4 M_\odot/L_\odot$ . To simulate SAURON observations, we combine pixels to obtain a minimum signal-to-noise (S/N), which we take proportional to the square root of the surface brightness. Adopting a typical mean error of  $7.5 \text{ km s}^{-1}$  in  $V$  and  $\sigma$ , and 0.03 for  $h_3$  through  $h_6$ , we assign per (Voronoi) bin an error, weighted with the S/N, and use these errors to (Gaussian) randomize the kinematic maps.

The resulting maps of the surface brightness,  $V$ ,  $\sigma$ ,  $h_3$  and  $h_4$  are shown in top rows in Figures 1–5 for each of the thirteen galaxy models, for which the specific choices are as follows.

*Fast rotator oblate models (FO1, FO2, FO3)* We choose the isochrone Stäckel potential so that the (mean) axis ratios of the corresponding density are  $p_S = 0.99$  and  $q_S = 0.76$ , such that the model is close to oblate axisymmetric<sup>1</sup>. The DF contains a NR and SR component with relative mass fractions of 30 and 70 per cent, and both with shape parameters  $w = u = -0.5$ . This results in regular velocity field around the (photometric) minor axis. From a luminosity weighted average of the simulated  $V$  and  $\sigma$  maps, we calculate the (projected) specific angular momentum  $\lambda_R = \langle R|V| \rangle / \langle R\sqrt{V^2 + \sigma^2} \rangle$  (see Emsellem et al. 2007). Both the edge-on and intermediate inclination models FO1 and FO2, have

$\lambda_R$  values of 0.36 and 0.33 that are well within the regime of the fast rotators. Even the close to face-on model FO3 has a  $\lambda_R$  value of 0.14 that is above the boundary  $\lambda_R = 0.10$  between fast and slow rotators.

*Slow rotator oblate models (SO1, SO2, SO3)* These three models are equivalent to the above fast rotator oblate models, except that the relative mass fractions of the DF components are inverted, i.e., 70 and 30 per cent for the NR and SR component, respectively. As a result, they rotate significant slower, with  $\lambda_R$  values for the edge-on, intermediate and face-on inclination models SO1, SO2 and SO3 of respectively 0.16, 0.15 and 0.06.

*Slow rotator prolate models (SP1, SP2, SP3)* The isochrone potential in this case is chosen such that the axis ratios of the corresponding density are  $p_S = 0.79$  and  $q_S = 0.78$ , i.e., close to prolate axisymmetric. The DF consists of a NR and LR component with relative mass fractions of 70 and 30 per cent, again both with shape parameters  $w = u = -0.5$ . The resulting kinematics show regular rotation around the (photometric) major axis. The amplitude of rotation is rather mild, with  $\lambda_R$  values for the side-on, intermediate and end-on models SP1, SP2 and SP3 of respectively 0.18, 0.15 and 0.05.

*Slow rotator triaxial models (ST1, ST2, ST3, ST4)* The axis ratios  $p_S = 0.90$  and  $q_S = 0.77$  of the density corresponding to the chosen isochrone potential are consistent with a triaxial model. Model ST1 only has a NR component with  $w = u = -0.5$ , and hence shows no rotation ( $\lambda_R = 0$ ), similar to NGC 4486 (M87). Model ST2 has an additional SR component with relative mass fraction of 20 per cent, so that  $\lambda_R = 0.14$ . Model ST3 has in addition to the NR component a SR component with relative mass fraction of 10 per cent and different shape parameters  $w = 0.5$  and  $u = -1.0$ . This results in a central compact kpc-size KDC and zero rotation outwards due to the extended NR component, similar to slow rotators like NGC 5831. The  $\lambda_R$  value within the inner  $10''$  rises above 0.10, but at larger radii quickly drops within the slow rotator regime. Finally, model ST4 is the same as model ST3, but with an additional LR component with  $u = w = -0.5$ . The three NR, SR and LR components have relative mass fractions of 80, 10 and 10 per cent. Outside the KDC, the model has significant (long-axis) rotation, similar to NGC 4365. As a result, the  $\lambda_R$  value stays around 0.10 in the outer parts.

Because the Abel models are constructed with a minimum number of DF components, they are transparent and relatively quick to calculate, but still they capture most of the rich dynamics observed in early-type galaxies. Moreover, a careful decomposition of the observed SAURON two-dimensional stellar kinematics of early-type galaxies using kinemetry shows that most early-type galaxies can be described by only a few components (Krajnović et al. 2008). Still, due to the sometimes sharp transition between the DF components, the surface brightness of the Abel models is not always as smooth as the surface brightness of most early-type galaxies. As a result, the surface brightness of the Abel models cannot accurately be fitted with smooth parameterizations such as the Multi-Gaussian Expansion method (MGE; Monnet et al. 1992; Emsellem et al. 1994), unless negative Gaussians and/or strong twists are invoked. This would not only be unnatural, but also incorrectly limit the possible deprojections. Nevertheless, the MGE parameterization allows for a straightforward deprojection and an efficient computation of the gravitational potential that correspond to the resulting (triaxial) intrinsic density. Therefore, we enforce a less accurate but smooth MGE parameterizations of the surface brightness of the Abel models, and show in § 4.4 that this does not affect our main results.

<sup>1</sup> In the axisymmetric limit the isochrone potential reduces to the Kuzmin & Kutuzov (1962) potential (cf. Dejonghe & de Zeeuw 1988).

### 3 CONSTRUCTING THE SCHWARZSCHILD MODELS

Based on the simulated observations of each of the thirteen Abel models, we now construct triaxial Schwarzschild (1979) models using our numerical code described in detail in vdB08. The code reconstructs the intrinsic dynamical structure of a collisionless stellar system with an arbitrary triaxial geometry by finding the superposition of orbits that best fits simultaneously the (observed) photometry and stellar kinematics in a self-consistent way. These models are significantly different from axisymmetric Schwarzschild models (e.g. van der Marel et al. 1998; Gebhardt et al. 2000; Valluri et al. 2004; Thomas et al. 2004; Cappellari et al. 2006), as they allow for triaxial intrinsic shapes and the associated multiple distinct orbit families. Hence, they are applicable to many of the early-type galaxies, including very boxy ones, and their triaxial dark haloes. The models presented in this paper use the default parameters as set in vdB08, including the number of orbits and the dimensions of the intrinsic polar mass grid. No regularisation was used throughout this paper, to ensure that the results unbiased towards any form of regularisation.

#### 3.1 Fitting the simulated observables of the Abel models

The stellar kinematics fitted are the maps of the mean line-of-sight velocity  $V$ , velocity dispersion  $\sigma$  and higher-order Gauss-Hermite velocity moments (up to  $h_6$ ) computed for each of the Abel models. In addition, we fit<sup>2</sup> the MGE parameterization of surface brightness distribution and the corresponding intrinsic luminosity density for a given viewing direction. Similarly, the intrinsic mass density and gravitational potential is inferred from the deprojected MGE parameterization of the surface mass distribution. Because the surface mass distribution is not directly observable (except perhaps in case of gravitational lensing), we constructed the Abel models such the luminosity density mimics the mass density inside the observed region (see § 2 and vdV08). Essentially, we implicitly assume that mass follows light. Unlike the sometimes sharp transitions in the projected luminosity density as mentioned in § 2, the projected mass density of the Abel models is always smooth and hence accurately parameterized by a MGE. The accelerations in the (efficiently) computed MGE gravitational potential are accurate to  $< 1\%$ , when compared to the input analytic Stäckel potential.

The types of orbits hosted by the gravitational potential depend strongly on the intrinsic shape of the galaxy. This means that the capability of the Schwarzschild models to fit the stellar kinematics (and the photometry in a self-consistent way) also depends on the intrinsic shape (see for example Fig. 5 of vdB08). To obtain the intrinsic density distribution from deprojection of the MGE parameterization three viewing angles are needed that are typically unknown: the polar ( $\vartheta$ ) and azimuthal ( $\varphi$ ) viewing angles, and the misalignment angle ( $\psi$ ) between the projected intrinsic short axis and the photometric minor axis.

Searching through a uniform grid in these three angles is unfeasible since the deprojection is strongly non-linear. While in parts of the grid small changes in the viewing angles can result in strong variations in the intrinsic shape, in other regions the intrinsic shape remains nearly constant. Instead, we step through the possible deprojections by regularly sampling three intrinsic shape parameters: the axis ratios  $p$  and  $q$ , and a third parameter  $u$  that represents the

scale-length compression factor. This has the advantage that we can sample the whole deprojection space with relatively few points and avoid sampling in parts of the viewing space where no changes occur, while increasing the sampling density where necessary (see also § 3.7 of vdB08). For the tests in this paper it is important to consider both the recovery of the viewing angles and the intrinsic shape separately. As a good constraint on the shape does not necessarily mean a good constraint on the viewing angles and vice versa.

The  $(p, q, u)$  parameters are not equivalent to the Stäckel  $p_S$  and  $q_S$  from § 2: both describe the intrinsic shape, but the latter describes the intrinsic shape measured directly from the moments of inertia in the isochrone Stäckel potential (see § 4.1 in vdV08), whereas  $(p, q, u)$  is defined within the MGE system.

The range of deprojections, and thus the sampling in the intrinsic shape parameters, is different for each of the galaxy models presented in this paper, as they have a different surface brightness. Typically we have 125 deprojections in steps of 0.05 in  $(p, q, u)$ , and for each deprojection we sample the mass-to-light ratio  $M/L$  at eleven different values. In this way, we construct around 1400 Schwarzschild models to the simulated observables of each Abel model. Computing the orbit library – which has to be done for every deprojection – takes approximately six hours on a current single-core CPU. For each deprojection and  $M/L$  the fitting takes another hour. This means in total about 2000 CPU hours to search the whole parameter space per Abel model.

#### 3.2 Confidence criterion

To determine the best-fit model parameters and corresponding uncertainties we compare for each Schwarzschild model its  $\chi^2$  difference between the simulated observables and the corresponding model predictions, weighted with the errors in the observables. The (global) minimum in the  $\chi^2$  yields the best estimate of the model parameters. It is common practice, e.g., when dynamical models are used to measure the mass of a black hole, to assign error bars based on  $\Delta\chi^2 = \chi^2 - \min(\chi^2)$  and the number of free parameters  $M$  of the model. In our case we have  $M = 4$  parameters (three viewing angles and the mass-to-light ratio) after marginalizing over the orbital weights. And thus our associated formal errors become  $\Delta\chi^2 = 4.72$  for 68% confidence ( $1\sigma$ ).

Whereas for the black hole mass measurements, with typically only a few observations inside the sphere of influence of the black hole, this works well, a different criterion is needed in our case of measuring the intrinsic shape based on (simulated) integral-field spectroscopy observations. The integral-field spectroscopy observations that are used typically consist of several hundred (or more) spectra. From each spectrum four (or more) velocity moments are extracted, yielding a large number of individual constraints  $N \gtrsim 10^4$ , which are fitted by the Schwarzschild model. Under these circumstances the uncertainties in the  $\chi^2$  itself become important. The  $\chi^2$  itself has a standard deviation of  $\sqrt{2(N - M)}$ , which becomes non-negligible in our case. Moreover, we expect that systematic errors in the observations (e.g. due to stellar template mismatch) can cause deviations in the  $\chi^2$  of the order of (or more than) the formal  $1\sigma$ .

Instead, we derive uncertainties on the best-fit parameters based on the expected standard deviation of  $\chi^2$ , which we approximate to be  $\sqrt{2N}$  because  $N \gg M$ . Preliminary validation of this approach is shown in vdB08, where we construct triaxial Schwarzschild models of one Abel model (similar to ST4) and the elliptical galaxy NGC 4365 with an (apparent) kinematically decoupled core. In this case and in the current study, the viewing angles of the Abel models

<sup>2</sup> Within the model the surface brightness and intrinsic density are actually treated as constraints instead of being directly fitted.

are known, so that this criterion for the standard error bars can be validated.

## 4 RESULTS OF THE DYNAMICAL MODELS

In Figures 1–5, we present for each Abel model the simulated observables, the best-fit Schwarzschild model, and the Schwarzschild model closest to the input parameters. The difference between the latter two Schwarzschild models reveals the (often small) differences due to the typical uncertainty allowed in the fitted stellar kinematics (e.g. template mismatch errors). The contour plots on the right indicate the confidence on the recovered M/L, the shape and the corresponding viewing angles. Besides the best-fit model (red crosses), they also show the location of the true input values (green diamonds). The white areas do not have a feasible deprojection. We first discuss the individual cases.

### 4.1 The oblate models

For all six oblate Abel models (SO1 through FO3) shown in Figures 1 and 2, the Schwarzschild models around the minimum in  $\chi^2$  are (very) good fits with reduced  $\chi^2$  per degrees-of-freedom close to unity. The shape is recovered well within the  $1\sigma$  confidence region. The edge-on and intermediate models (SO1, SO2, FO1, FO2) have a strong constraint on  $p > 0.95$ , fully excluding strongly triaxial geometries, while  $q$  is generally unconstrained, apart from the lower limit  $q > 1 - \varepsilon$  implied by the largest value of the observed ellipticity  $\varepsilon$ . Hence, we cannot constrain the inclination of these (near) axisymmetric systems. The differences in the fitted kinematics between the best-fitting model and the model with the correct input parameters (see Fig. 1) are so small that they are negligible compared to possible (systematic) errors in real observations.

As expected, the face-on slow-rotator model SO3 has the worst recovery with no significant constraint on its shape and a wide range in M/L allowed. All the other oblate models have a constraint on M/L that is consistent with the input value. The constraints on all the fast-rotator oblate models are tighter than those on the slow-rotator oblate models because the mean velocity amplitude in the fast-rotator models is larger, which effectively shrinks the simulated observational errors.

For all oblate models the flattening  $q$  of the best-fit model is never far removed from the input value  $q_0$ :  $\Delta q \equiv |q - q_0| < 0.08$ . Even though the viewing direction, or the inclination in this case, is mostly unconstrained, the latter indicates that the intrinsic shape is not fully degenerate. Observations that are more accurate and/or span a larger field-of-view are expected to yield tighter constraints on the intrinsic shape. When we fitted the surface brightness of the Abel models directly instead of the overly smooth MGE parameterization, the constraints on the shape improve, but only mildly, showing that our MGE parameterization is sufficient for the oblate models.

### 4.2 The prolate models

The results for the (slow-rotator) prolate models (SP1, SP2, SP3) are shown in Fig. 3. The constraint on the shape is better than for the oblate models and the true shapes and M/L lie within or on the  $1\sigma$  confidence contour. In all cases the axis ratios are well recovered with allowed ranges  $\Delta p < 0.07$  and  $\Delta q < 0.07$ . Even the end-on model SP3 has a good constraint on the shape, excluding more than 75% of the allowed range in  $p$  and  $q$ . The constraint on the shape for prolate systems is better than for the oblate systems due to the fact

that there are less (near) prolate deprojections possible than oblate ones. Similarly, the limits on the inclination from the photometry are more restrictive in the prolate than oblate case, but still the regular kinematics do not really further constrain the inclination.

### 4.3 The triaxial models

Model ST1 (Fig. 1) is a non-rotating round galaxy seen at an intermediate viewing angle. Like the face-on slow-rotator oblate model SO3 - which shows almost no rotation - the triaxial Schwarzschild models are capable of reproducing all features in the simulated observables at nearly all viewing angles. The M/L is recovered with a similar accuracy as in the case of the oblate models, despite the lack of constraint on the intrinsic shape. Even so, the best-fit  $p$  and  $q$  are with 10 per cent from the input values, while the formally allowed ranges are larger with  $\Delta p \sim 0.30$  and  $\Delta q \sim 0.30$ .

The zero velocity curve of the stellar kinematics in model ST2 seen in Fig. 4 is twisted with respect to the photometric minor axis. Since this is only possible in a non-axisymmetric system, we might expect a rather good recovery of the intrinsic shape. However, the constraints are not very good with ranges  $\Delta p \sim 0.15$  and  $\Delta q \sim 0.25$ , and comparable with those on the shape of the slow rotator oblate models SO1 and SO2. Model ST3 (Fig. 4) has a central rotating component and no rotation in the outer parts. The resulting constraint on the intrinsic shape with ranges  $\Delta p \sim 0.15$  and  $\Delta q \sim 0.20$  is only slightly better than model ST2. However, as we show below in § 4.4 and in Fig. 6, taking into account the strong photometric twist improves the recovery of the intrinsic shape as well as the (weak) constraint on the viewing angles.

Model ST4 (Fig. 5) contains a central KDC like model ST3, and additionally shows significant rotation in the outer parts. Although the inner part of the surface brightness is not well reproduced by the smooth MGE parameterization, unlike model ST3, the intrinsic shape is nevertheless accurately recovered and constrained, with ranges  $\Delta p < 0.05$  and  $\Delta q < 0.05$ . The triaxial Abel model used in vdB08 and vdV08 is similar to model ST4, but at a different viewing direction and with more photometric twist in the MGE parameterization, resulting in (slightly) tighter constraints on the intrinsic shape as well as on the viewing angles.

### 4.4 Fitting the non-smooth surface brightness directly

As mentioned in § 2, the surface brightness of the Abel models can show a sudden transition between DF components, which cannot be accurately described by a smooth MGE parameterization without invoking negative Gaussians and/or strong photometric twists. A way to avoid this is to bypass the MGE and use the observed surface brightness directly. This means that the intrinsic density is not constrained anymore, since it follows from deprojecting the MGE parameterization. In Fig. 6, we present the results for model ST3, which shows most evidently both a central depression as well as a strong photometric twist in its surface brightness. The intrinsic shape is still correctly recovered, but now the best-fit model is much closer to the input values. Also many of the deprojections with  $p > 0.93$  or  $q > 0.67$  are excluded, leading to a significantly tighter constraint on the intrinsic shape than when the MGE parameterization is used. In Fig. 6 we also show the same for ST2, for which the effect is less pronounced but still significant: the best-fit model is now much closer with  $p$  and  $q$  less than 0.05 away from their input values, but the confidence intervals are unchanged.

This shows that the MGE representation we used in § 4.3 is too

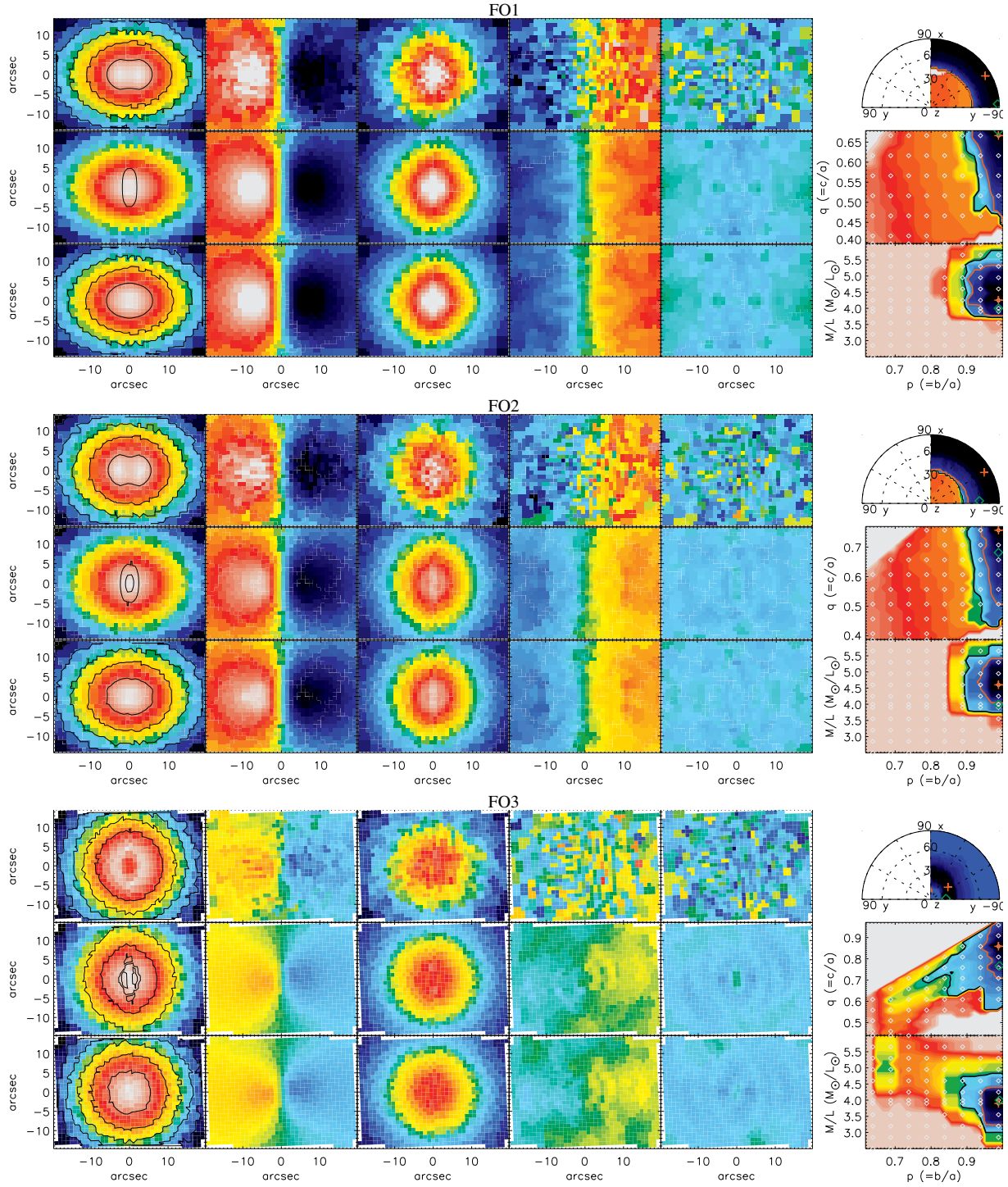


**Figure 1.** Dynamical modelling of fast rotator oblate models FO1, FO2 and FO3. Each plot shows the stellar kinematics of the Abel model (top), the best-fit Schwarzschild model (middle), and the fit at the input parameters (bottom). The contours on the surface brightness image (leftmost panel) show the observed surface brightness (top), the surface brightness of the MGE model (bottom) and the difference between the two (middle). Columns 2 through 5 show the line-of-sight velocity moments:  $V$  ( $-110 \dots 110 \text{ km s}^{-1}$ ),  $\sigma$  ( $100 \dots 260 \text{ km s}^{-1}$ ),  $h_3$  and  $h_4$  ( $-0.1 \dots 0.1$ ). The panels on the right side show marginalized confidence regions of the viewing angles  $\vartheta$  and  $\varphi$  (in Lambert projection seen down the  $z$ -axis, so that  $\vartheta$  runs radially and  $\varphi$  runs azimuthally),  $p$  versus  $q$ , and  $p$  versus  $M/L$ . The inner red and outer black contour signify  $1\sigma$  and  $3\sigma$  confidence, respectively. The red cross and green diamond highlight the best-fit parameters and the original input parameters, respectively.



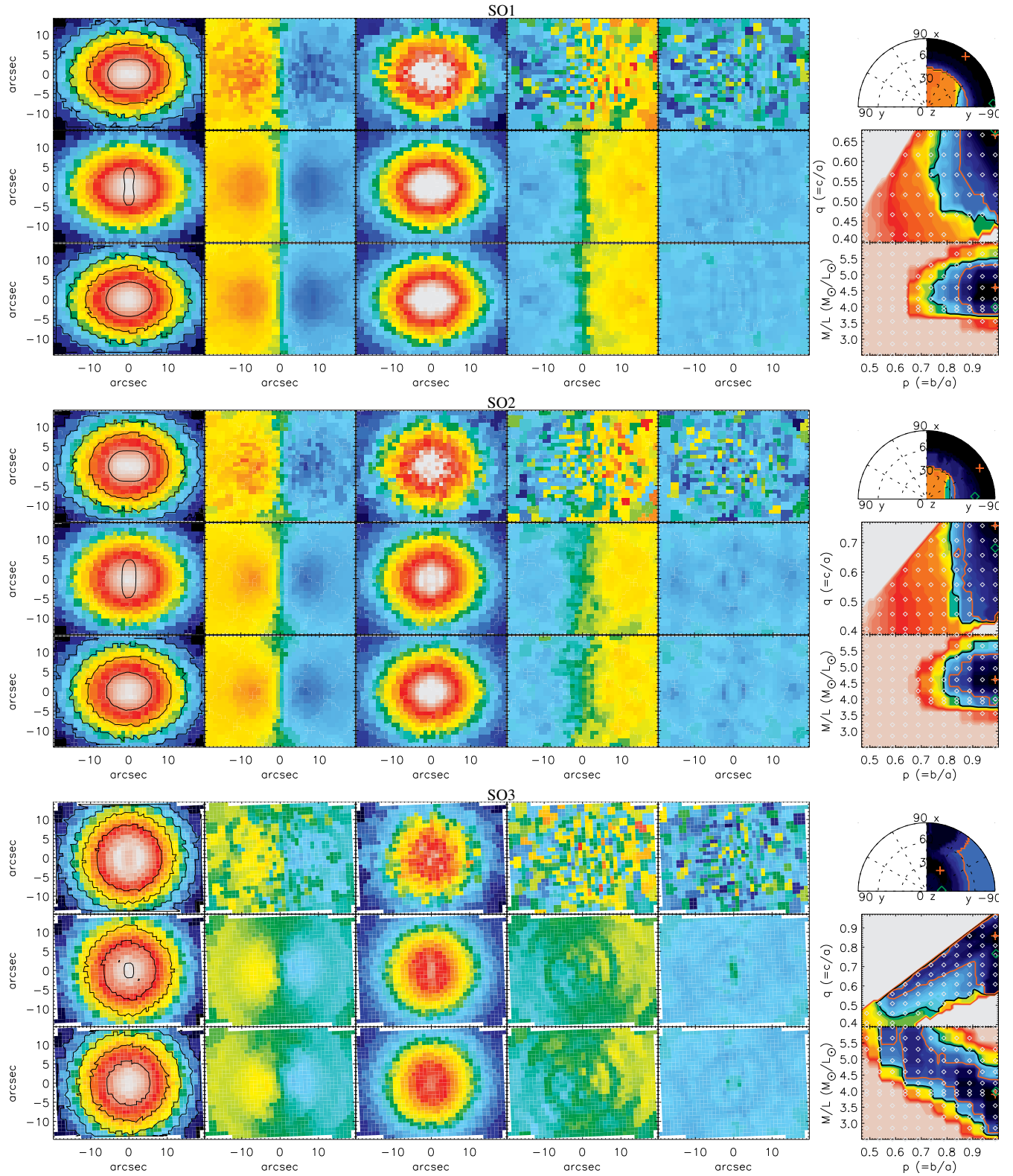
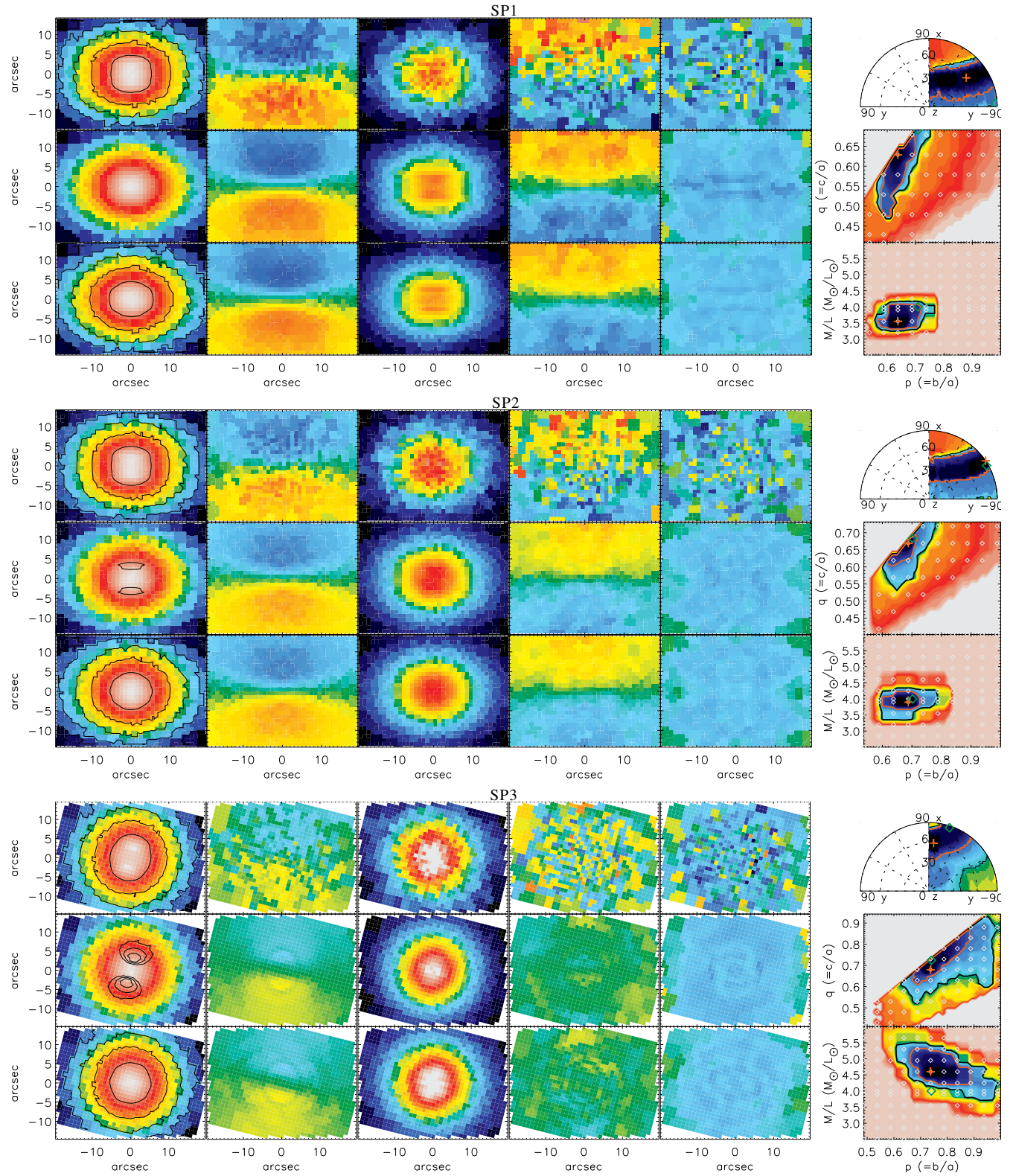
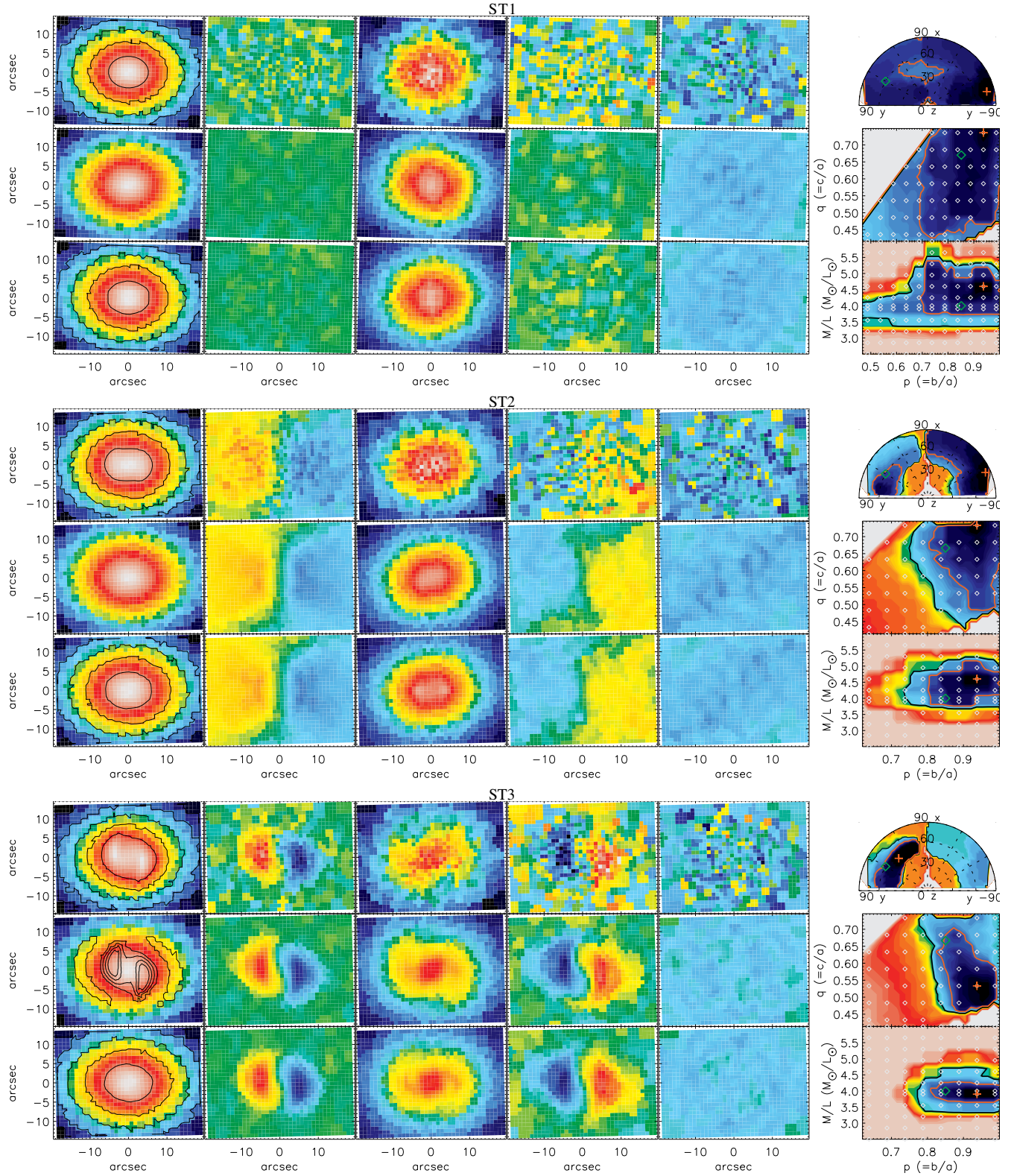


Figure 2. Slow rotator oblate models SO1, SO2 and SO3. See Fig. 1 for description.



**Figure 3.** Slow rotator prolate models SP1, SP2 and SP3. See Fig. 1 for description.





**Figure 4.** Slow rotator triaxial models ST1, ST2 and ST3. See Fig. 1 for description.

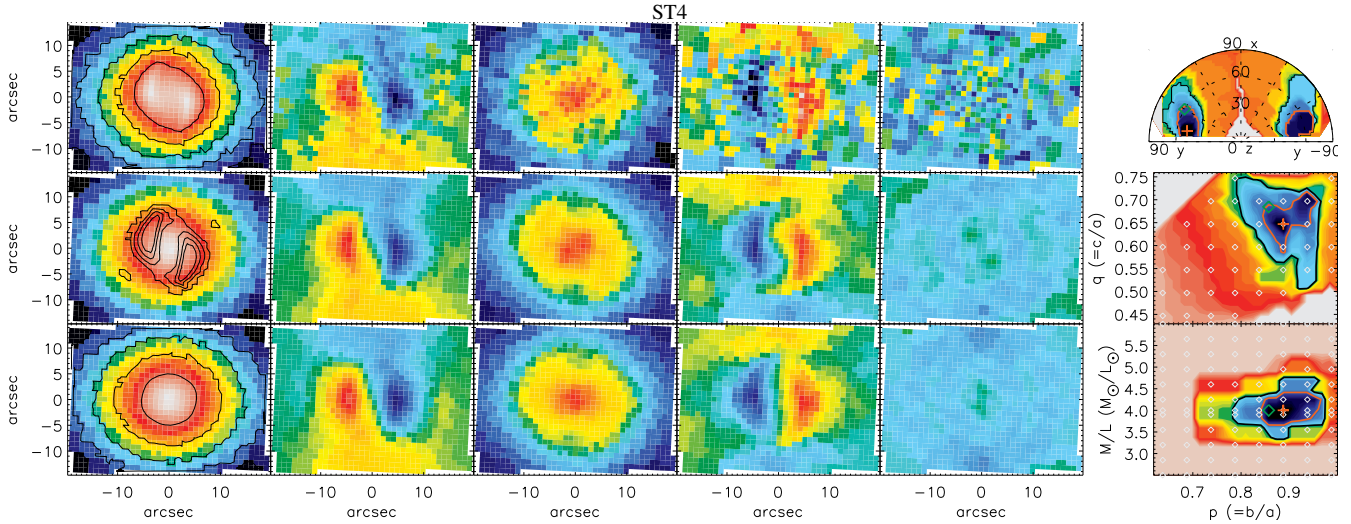


**Figure 5.** Slow rotator triaxial model ST4. See Fig. 1 for description.

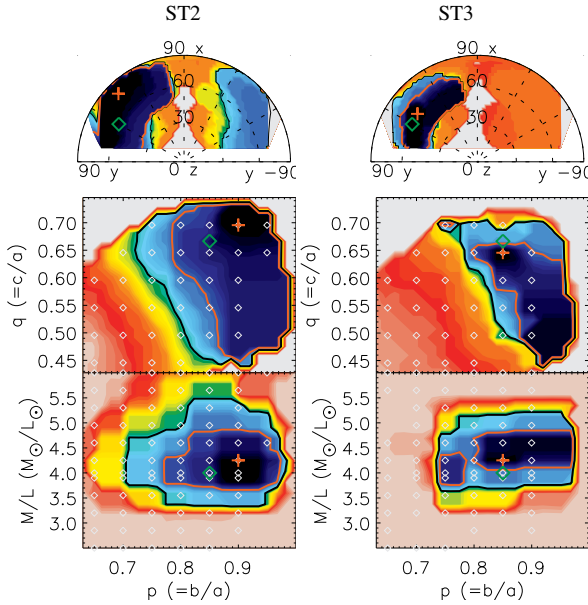


**Figure 6.** The shape recovery of model ST2 (left) and ST3 (right), when the observed surface brightness is fitted directly, bypassing the (too) smooth MGE parameterization. The presentation of the models here is identical to the ones in in Fig. 4.

smooth, adding irrelevant deprojections that (artificially) increase the error bars on  $p$  and  $q$ . However, there is a delicate balance between reproducing too little and too much photometric twist. Fitting unrealistic sharp features (due to for example dust in real observations), may exclude allowed deprojections or even the true underlying intrinsic shape. To avoid the latter, the fit to the surface brightness should be as round as possible, while still accurately describing the observed photometry.

## 5 INTRINSIC VELOCITY MOMENTS

In vdV08, we have shown that given the correct input viewing direction, the internal dynamics and three-integral distribution function can be recovered. Here, we investigate what happens to the intrinsic

velocity moments when the viewing angles are allowed to deviate from the input values. We expect the intrinsic velocity moments, in terms of  $V/\sigma$  and velocity anisotropy, to vary when the viewing direction and hence intrinsic shape changes. Still, if we stay within the  $1\sigma$  confidence regions of the fitted intrinsic shape parameters, these variations might be limited due to the constraints coming from the two-dimensional kinematics. We use model ST3 from the previous section as an illustration. In Fig. 7, we show the intrinsic velocity moments at the input values  $(p, q) = (0.85, 0.66)$  and at  $(p, q) = (0.90, 0.50)$ , which is at the (lower) boundary of the corresponding  $1\sigma$  confidence region (see also Fig. 6). While the mass density of the two models (indicated by the black contours) is clearly different, the intrinsic velocity moments are quite similar. This suggests that as long as the intrinsic shape is reasonably well constrained, the internal dynamics are also reliably recovered.

## 6 DISCUSSION AND CONCLUSIONS

We constructed thirteen galaxy models with simulated photometry and two-dimensional stellar kinematics that represent the SAURON observations of early-type galaxies, from oblate fast rotator to triaxial slow rotator. We fitted realistic three-integral triaxial Schwarzschild models to the simulated observables of these Abel models and we used the  $\chi^2$  difference to investigate how well the intrinsic shape as well as the mass-to-light ratio can be recovered. Due to the large number of observational constraints (typically  $N > 10^4$ ) with possible systematic errors (e.g. stellar template mismatch) in the case of real integral-field observations, the commonly used  $\Delta\chi^2 = \chi^2 - \min(\chi^2)$  is not useful to estimate the uncertainties on the model parameters. Instead, we showed that the standard deviation  $\sqrt{2N}$  works well as a confidence criterion.

The simulated observations of the (near) oblate Abel models that are not viewed close to face-on strongly excluded triaxial intrinsic shapes with  $1 - p < 0.05$ . The flattening  $q$  is almost only constrained by the photometry, although the models with more projected rotation provide a slightly tighter constraint since the relative errors in the odd velocity moments are smaller. This means that for fast-rotator early-type galaxies, which seem to be consistent with oblate axisymmetry, the inclination is not significantly further constrained by current two-dimensional stellar kinematics, consistent



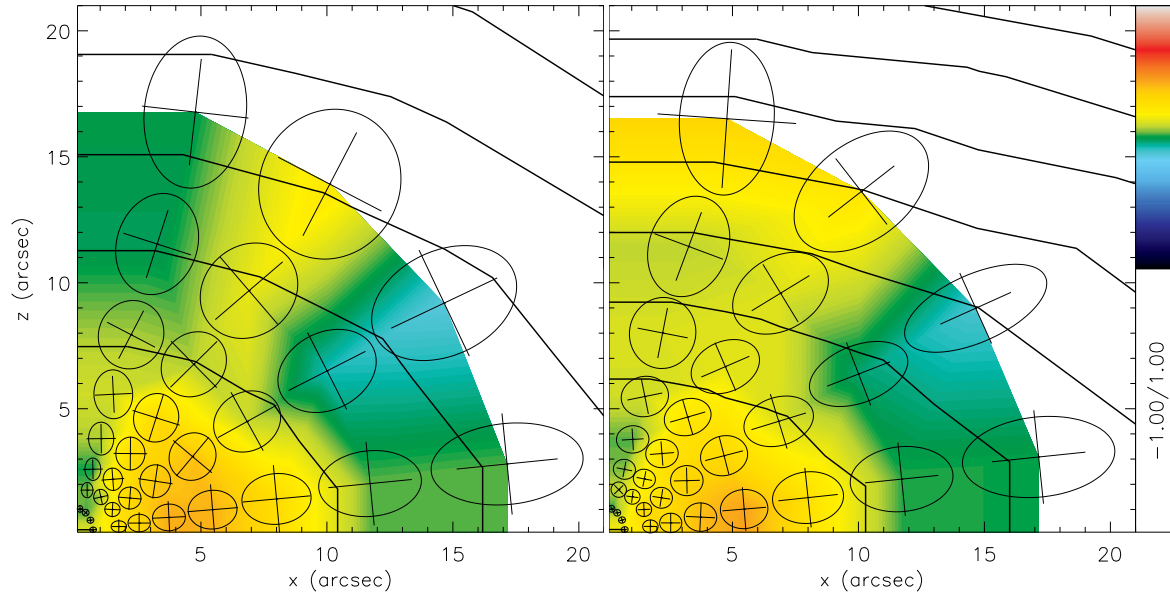


**Figure 7.** The intrinsic velocity moments of triaxial Schwarzschild models fitted to the simulated observables of the Abel model ST3. In the left panel, the intrinsic shape parameters are at the true input values, while in the right panel they are at the boundary of the corresponding  $1\sigma$  confidence region. The colour represents the (intrinsic)  $V/\sigma$ , and the ellipses are cross-sections of the velocity ellipsoid with the  $(x, z)$  plane, while the crosses indicate the (relative) size of the velocity ellipsoid in the perpendicular ( $y$ -axis) direction (see § 5.3 of vdV08 for further details). The black curves are contours of constant mass density in steps of 1 mag.

with Krajnović et al. (2005). Similarly, for the (near) prolate Abel models that are not viewed close to end-on a triaxial intrinsic shape is strongly excluded with  $p - q < 0.05$ , but the viewing direction is only weakly constrained.

Unlike axisymmetric galaxies, a triaxial galaxy can show twists in both the surface brightness and velocity field (and in higher-order velocity moments), as well as misalignment between the kinematic (rotation) axis and the photometric minor axis. The stronger such features are in the observations, the more accurate the intrinsic triaxial shape can be recovered, often better than in the axisymmetric case. In particular, for the triaxial Abel models with a central KDC,  $p$  and  $q$  can be recovered within 5%, especially when (misaligned) rotation is present in the outer parts. Since such kpc-size KDCs seem typical for the slow-rotator early-type galaxies, we expect that their intrinsic shape can be well estimated from dynamical modeling. However, when inferring the mass model from a fit to the surface brightness, the fit should be as round as possible to not exclude allowed deprojections, but still accurately describe the photometry, including twists, to avoid artificially increasing the range of allowed intrinsic shapes.

Near face-on oblate galaxies and end-on prolate galaxies appear round on the sky and show almost no (projected) rotation. We showed that in these cases, as well as for triaxial galaxies with no intrinsic (net) rotation, the best-fit  $p$  and  $q$  are still remarkably close to their true values (typically within 10%), but the formal uncertainties are much larger (typically around 30%). This means that for galaxies that appear round on the sky and show little rotation, the only hope of recovering the intrinsic shape and corresponding viewing direction is through additional constraints such as provided by a thin embedded disc (in either dust, gas or stars).

In all cases, the  $M/L$  is correctly recovered, within about 10% when the intrinsic shape is well recovered, increasing up to 20% for the models with a poor constraint on the intrinsic shape. This is in line with Thomas et al. (2007), who showed that applying

axisymmetric Schwarzschild models to triaxial merger remnants results in a larger scatter in the recovered  $M/L$  compared to oblate remnants. However, as long as generic dynamical models such as our triaxial Schwarzschild models are used, the recovery of the  $M/L$  is nearly independent of the underlying intrinsic shape. This is not unexpected given the good correlation between dynamical and virial  $M/L$  estimates (e.g. Cappellari et al. 2006), and the observed tight scaling relations in early-type galaxies such as the fundamental plane (e.g. Dressler et al. 1987; Djorgovski & Davis 1987).

In real galaxies the photometry and the kinematics are usually measured independently and as a result their relative alignment is not perfectly known. This can create a small kinematic misalignment in an otherwise perfectly axisymmetric galaxy, or vice-versa. To test the significance of this we re-ran the fast rotator oblate model FO2 with a positive and negative misalignment of  $2^\circ$ , emulating a typical measurement error on the PA (in a fairly round galaxy). The resulting recovered parameters and their errors were very similar to the original FO2 model, with the  $\chi^2$  only marginally higher and the  $3\sigma$  confidence region slightly extended. This shows that the uncertainty in the relative PA in these observations does not effect the recovery of the intrinsic shape nor the recovery of the mass-to-light ratio.

Furthermore, we ran separate models of FO2 and ST4 in which we doubled the number of orbits. The resulting models, including the  $\chi^2$  contours and the recovered kinematics, were nearly identical showing that the number of orbits used in our models is sufficient.

We conclude that for (near) axisymmetric galaxies the combination of photometric and two-dimensional stellar kinematic observations can strongly exclude triaxiality, but regular kinematics do not further tighten the intrinsic flattening significantly. As a result, we expect the inclination of fast-rotator early-type galaxies to remain nearly unconstrained above the photometric lower limit, although better observations do seem to slightly decrease the range in inclinations (§4.1). Triaxial galaxies can have additional complexity

in both the observed photometry and kinematics, such as the central KDCs observed in many slow-rotator early-type galaxies, which allows the intrinsic shape to be accurately recovered. The intrinsic shape of round galaxies with no significant rotation is degenerate, unless additional constraints such as from a thin disk are available.

## ACKNOWLEDGMENTS

We thank Anne-Marie Weijmans and Tim de Zeeuw for useful comments on the manuscript, and Michele Cappellari for many lively discussions. RvdB acknowledges support from grant 614.000.301 from NWO and the LKBF. GvdV acknowledges support provided by NASA through Hubble Fellowship grant HST-HF-01202.01-A awarded by the Space Telescope Science Institute, which is operated by the Association of Universities for Research in Astronomy, Inc., for NASA, under contract NAS 5-26555. This paper uses software from Cappellari (2002), Cappellari & Copin (2003) and Gould, Orban & Toint (2003).

## REFERENCES

- Binney J., 1985, *MNRAS*, 212, 767
- Binney J., Mamon G. A., 1982, *MNRAS*, 200, 361
- Cappellari M., 2002, *MNRAS*, 333, 400
- Cappellari M., 2008, *MNRAS*, 390, 71
- Cappellari M., Bacon R., Bureau M., Damen M. C., Davies R. L., de Zeeuw P. T., Emsellem E., Falcón-Barroso J., Krajnović D., Kuntschner H., McDermid R. M., Peletier R. F., Sarzi M., van den Bosch R. C. E., van de Ven G., 2006, *MNRAS*, 366, 1126
- Cappellari M., Copin Y., 2003, *MNRAS*, 342, 345
- Chakraborty D. K., Singh A. K., Gaffar F., 2008, *MNRAS*, 383, 1477
- Davies R. L., Kuntschner H., Emsellem E., Bacon R., Bureau M., Carollo C. M., Copin Y., Miller B. W., Monnet G., Peletier R. F., Verolme E. K., de Zeeuw P. T., 2001, *ApJ*, 548, L33
- Dejonghe H., 1986, *Phys. Rep.*, 133, 217
- Dejonghe H., de Zeeuw T., 1988, *ApJ*, 329, 720
- Dejonghe H., Laurent D., 1991, *MNRAS*, 252, 606
- Djorgovski S., Davis M., 1987, *ApJ*, 313, 59
- Dressler A., Lynden-Bell D., Burstein D., Davies R. L., Faber S. M., Terlevich R., Wegner G., 1987, *ApJ*, 313, 42
- Emsellem E., Cappellari M., Krajnović D., van de Ven G., Bacon R., Bureau M., Davies R. L., de Zeeuw P. T., Falcón-Barroso J., Kuntschner H., McDermid R., Peletier R. F., Sarzi M., 2007, *MNRAS*, 379, 401
- Emsellem E., Cappellari M., Peletier R. F., McDermid R. M., Bacon R., Bureau M., Copin Y., Davies R. L., Krajnović D., Kuntschner H., Miller B. W., de Zeeuw P. T., 2004, *MNRAS*, 352, 721
- Emsellem E., Monnet G., Bacon R., 1994, *A&A*, 285, 723
- Franx M., Illingworth G., de Zeeuw P. T., 1991, *ApJ*, 383, 112
- Gebhardt K., Richstone D., Kormendy J., Lauer T. R., Ajhar E. A., Bender R., Dressler A., Faber S. M., Grillmair C., Magorrian J., Tremaine S., 2000, *AJ*, 119, 1157
- Gerhard O. E., 1993, *MNRAS*, 265, 213
- Gould N. I. M., Orban D., Toint P. L., 2003, *ACM Transactions on Mathematical Software*, 29(4), 353
- Hunter C., de Zeeuw P. T., 1992, *ApJ*, 389, 79
- Jing Y. P., Suto Y., 2002, *ApJ*, 574, 538
- Kormendy J., Bender R., 1996, *ApJ*, 464, L119+
- Krajnović D., Bacon R., Cappellari M., Davies R. L., de Zeeuw P. T., Emsellem E., Falcón-Barroso J., Kuntschner H., McDermid R. M., Peletier R. F., Sarzi M., van den Bosch R. C. E., van de Ven G., 2008, *MNRAS*, 390, 93
- Krajnović D., Cappellari M., Emsellem E., McDermid R. M., de Zeeuw P. T., 2005, *MNRAS*, 357, 1113
- Kuzmin G. G., Kutuzov S. A., 1962, *Bull. Abastumani Astroph. Obs.*, 27, 82
- Lambas D. G., Maddox S. J., Loveday J., 1992, *MNRAS*, 258, 404
- Mathieu A., Dejonghe H., 1999, *MNRAS*, 303, 455
- Merritt D., 1985, *AJ*, 90, 1027
- Monnet G., Bacon R., Emsellem E., 1992, *A&A*, 253, 366
- Osipkov L. P., 1979, *Pis'ma v Astronomicheskii Zhurnal*, 5, 77
- Padilla N. D., Strauss M. A., 2008, *MNRAS*, 388, 1321
- Rybicki G. B., 1987, in de Zeeuw P. T., ed., *IAU Symp. 127: Structure and Dynamics of Elliptical Galaxies*. p. 397
- Ryden B., 1992, *ApJ*, 396, 445
- Ryden B. S., 1996, *ApJ*, 461, 146
- Schwarzschild M., 1979, *ApJ*, 232, 236
- Statler T. S., 1994, *AJ*, 108, 111
- Tenjes P., Busarello G., Longo G., Zaggia S., 1993, *A&A*, 275, 61
- Thomas J., Jesseit R., Naab T., Saglia R. P., Burkert A., Bender R., 2007, *MNRAS*, 381, 1672
- Thomas J., Saglia R. P., Bender R., Thomas D., Gebhardt K., Magorrian J., Richstone D., 2004, *MNRAS*, 353, 391
- Valluri M., Merritt D., Emsellem E., 2004, *ApJ*, 602, 66
- van de Ven G., de Zeeuw P. T., van den Bosch R. C. E., 2008, *MNRAS*, 385, 614, (vdV08)
- van den Bosch R. C. E., van de Ven G., Verolme E. K., Cappellari M., de Zeeuw P. T., 2008, *MNRAS*, 385, 647, (vdB08)
- van der Marel R. P., Cretton N., de Zeeuw P. T., Rix H., 1998, *ApJ*, 493, 613
- van der Marel R. P., Franx M., 1993, *ApJ*, 407, 525
- Verolme E. K., Cappellari M., Copin Y., van der Marel R. P., Bacon R., Bureau M., Davies R. L., Miller B. M., de Zeeuw P. T., 2002, *MNRAS*, 335, 517
- Williams T. B., 1981, *ApJ*, 244, 458

This paper has been typeset from a  $\text{\LaTeX}$  file prepared by the author.